

# Facile Growth of Barium Oxide Nanorods: Structural and Optical Properties

Naushad Ahmad<sup>1,\*</sup>, Rizwan Wahab<sup>2,\*</sup>, and Manawwer Alam<sup>3</sup>

<sup>1</sup>Department of Chemistry, College of Science, King Saud University, Riyadh 11451, Kingdom of Saudi Arabia

<sup>2</sup>College of Science, Department of Zoology, King Saud University, Riyadh 11451, Kingdom of Saudi Arabia

<sup>3</sup>Research Centre, College of Science, King Saud University, P.O. Box-2455, Riyadh 11451, Kingdom of Saudi Arabia

This paper reports a large-scale synthesis of barium oxide nanorods (BaO-NRs) by simple solution method at a very low-temperature of  $\sim 60$  °C. The as-grown BaO-NRs were characterized in terms of their morphological, structural, compositional, optical and thermal properties. The morphological characterizations of as-synthesized nanorods were done by scanning electron microscopy (SEM) which confirmed that the synthesized products are rod shaped and grown in high density. The nanorods exhibits smooth and clean surfaces throughout their lengths. The crystalline property of the material was analyzed with X-ray diffraction pattern (XRD). The compositional and thermal properties of synthesized nanorods were observed via Fourier transform infrared (FTIR) spectroscopy and thermogravimetric analysis which confirmed that the synthesized nanorods are pure BaO and showed good thermal stability. The nanorods exhibited good optical properties as was confirmed from the room-temperature UV-vis spectroscopy. Finally, a plausible mechanism for the formation of BaO-NRs is also discussed in this paper.

**Keywords:** Chemical Synthesis, Barium Oxide, Nanorods, Structural Properties, Optical Properties.

## 1. INTRODUCTION

Metal oxide nanomaterials are considered as one of the richest nanomaterials family because of its growing research and versatile applications.<sup>1–10</sup> The oxide nanomaterials are widely used for variety of applications such as sensors, actuators, capacitors, biomedical sciences, environmental sciences, solar cells, Li-ion batteries and so on. Due to the versatile applications of this class of material, extensive researches have been done in this area and reported in the literature. Traditionally, synthetic approaches for the production of functional metal oxide materials have involved high temperature reactions with energy intensive techniques.<sup>1</sup> However, the high-temperature growth involves various sophisticated synthetic techniques such as laser ablation, ion implantation, chemical vapor deposition, thermal decomposition, thermal evaporation, plasma enhanced chemical vapor deposition and so on.<sup>1–11</sup> Due to high-temperature and high cost growth of these nanomaterials, much efforts have

been done to decrease the synthesis temperature and cost. The solution technique provides a cost effective and facile way to synthesize metal oxide nanomaterials in large quantity.

Among various metal oxide nanomaterials, the barium oxide nanostructures possess a particular place due to its own properties and wide applications. Using barium oxide nanoparticles, researchers have developed a self-cleaning technique that could allow solid oxide fuel cells to be powered directly by coal gas at operating temperatures as low as 750 °C.<sup>1</sup> The technique could provide a cleaner and more efficient alternative to conventional power plants for generating electricity from the nation's vast coal reserves. Barium oxide is a hygroscopic material (it absorbs water) and the researchers have taken advantage of this material to enable chemical reactions to take place on the surface of anode by depositing barium oxide nanostructures on their surface. The nanoparticles promote the oxidation of the carbon deposits (to CO<sub>2</sub>) and keep the anode surface clean.<sup>1</sup> It is well known that the physical properties of nanoparticles are dependents on microstructure, e.g., grain

\* Authors to whom correspondence should be addressed.

boundaries, point and extended defects, as well as surface morphology. Therefore, it is considered important to investigate the microstructure of barium oxide nanoparticles to obtain a better understanding of size effects on the physical properties.

This paper reports the facile growth and characterization of barium oxide nanorods prepared through simple solution process at low-temperature of  $\sim 60$  °C. The synthesized nanorods were examined by various analytical techniques such as SEM, EDS, XRD, FTIR, UV and TGA. Finally, a plausible mechanism for the formation of these nanorods has been proposed based on the chemical reaction involve during the synthesis process.

## 2. EXPERIMENTAL DETAILS

### 2.1. Material Synthesis

Barium oxide (BaO) nanorods were synthesized by facile and simple solution process by using barium nitrate hexahydrate ( $\text{Ba}(\text{NO}_3)_2 \cdot 6\text{H}_2\text{O}$ ), sodium hydroxide (NaOH) and hydrazine ( $\text{N}_2\text{H}_4$ ). All the chemicals used for the synthesis were purchased from Sigma-Aldrich and used as-received without further purification. In a typical reaction process, 0.1 M of  $\text{Ba}(\text{NO}_3)_2 \cdot 6\text{H}_2\text{O}$  and 0.1 M hydrazine, both dissolved in 100 ml de-ionized (DI) water, were mixed together under continuous stirring for 20 min. Consequently, 0.1 M NaOH, made in DI water, was added to the resultant solution until the solution  $\text{pH} = 12$  and stirred for 30 min at room-temperature. After stirring, the resultant solution was refluxed at 60 °C for 3 h in a two-necked refluxing pot. After refluxing, the refluxing pot was naturally cooled to room-temperature. White precipitate was obtained which was washed with DI water and ethanol several times and dried at room-temperature. The as-synthesized powder was then characterized in terms of their morphological, structural, compositional and optical properties.

### 2.2. Characterization

The morphological observations of the white powder were made by a scanning electron microscope (SEM). For SEM observations, the powder was uniformly sprayed onto carbon tape and examined. The crystallinity and phases of the white powders were characterized by X-ray powder diffractometer (XRD) with  $\text{Cu-K}\alpha$  radiation ( $\lambda = 1.54178$  Å) in the range of 20–60° with 6 °/min scanning speed. The thermal analysis (TGA) was performed using TA instruments (SDT Q-600, U.S.A). For thermal analysis, about 5 mg of the sample was loaded into alumina crucibles ( $\text{Al}_2\text{O}_3$ ) in the heating zone of the TGA. An empty pan was used as reference. The thermal scanning mode ranges from ambient temperature to 800 °C at a programming heating rate of 20 °C/min under helium gas with a gas flow of 100 ml/min. The chemical compositions of the synthesized white powder was examined by using Fourier transform infrared (FTIR; PerkinElmer-FTIR Spectrum-100) in the range of

400–4000  $\text{cm}^{-1}$ . The optical property of the prepared sample was studied by UV-visible (UV-vis, Shimadzu Japan), in the range from 250–600 nm at room temperature.

## 3. RESULTS AND DISCUSSION

### 3.1. Scanning Electron Microscopy (SEM)

The general morphologies of as-synthesized barium oxide nanorods were examined by SEM and shown in Figures 1(a)–(d). The low-magnification images reveal that the synthesized products are rod-shaped and grown in large-quantity (Figs. 1(a) and (b)). It is clear from the micrographs that due to high-density growth, the nanorods are accumulated and two or more rods are joined each other. From the high-resolution images, it is clear that the nanorods are possessing smooth and clean surfaces throughout their lengths (Figs. 1(c) and (d)). The typical diameters of the nanorods are in the range 250–300 nm with lengths of 5–6  $\mu\text{m}$ . The elemental composition of as-synthesized nanorods were examined by energy dispersive spectroscopy (EDS) attached with SEM. The observed EDS spectrum (not shown here) confirms that the synthesized nanorods are barium oxide without any significant impurity.

### 3.2. X-Ray Diffraction (XRD)

To examine the crystallinity and crystal phases, the as-synthesized barium oxide nanorods were examined by X-ray diffraction pattern, measured with  $\text{Cu-K}\alpha$  radiations in the range of 20–60° with 6 °/min scanning speed. Figure 2 exhibits the typical X-ray diffraction pattern of as-synthesized BaO. Several well-defined peaks correspond to various planes of BaO were seen in the observed XRD pattern which are all related and well matched with the phase of pure well-crystalline BaO.<sup>11, 12</sup> The observed diffraction reflections of BaO are appeared at 34.12°, 42.16°, 44.65° and 46.86° which are correspond to the (104), (204), (302) and (312) planes, respectively of BaO. The observed results are well matched with the reported literature.<sup>11, 12</sup>

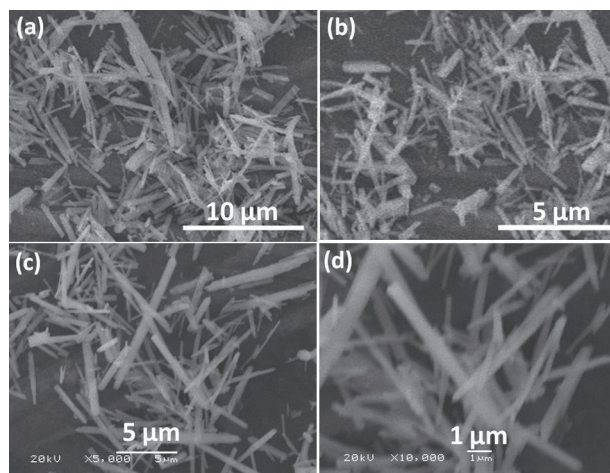


**Figure 1.** Typical (a) and (b) low-magnification and (c) and (d) high-resolution SEM images of as-synthesized Barium oxide nanorods.

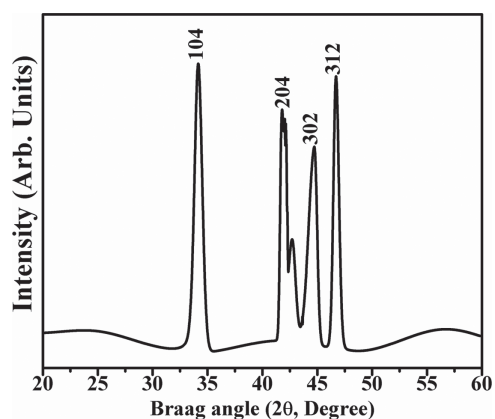


**Figure 2.** Typical X-ray diffraction pattern of as-synthesized Barium oxide nanorods.

### 3.3. FTIR Spectrum

To examine the chemical composition and purity of as-synthesized BaO-NRs, FTIR was done in the range of 4000–400  $\text{cm}^{-1}$  and results are demonstrated in Figure 3. The observed FTIR spectrum shows a well-defined band at 695  $\text{cm}^{-1}$  which was originated due to the formation of metal–oxygen (Ba–O) bond. In addition of Ba–O bond, two bands appeared at  $\sim 1630 \text{ cm}^{-1}$  and  $\sim 3467 \text{ cm}^{-1}$  in the spectrum are related with the O–H stretching and bending modes of vibrations, respectively. The peak originated at 856  $\text{cm}^{-1}$  is related with the asymmetric vibration of  $\text{NO}_3^{-1}$  ions.<sup>13–15</sup> The obtained results are consistent with the already reported literature.<sup>13–15</sup> No other band related with any other functional group was detected in the FTIR spectrum which reveals that the as-synthesized BaO nanorods possess good purity without any significant impurity.

### 3.4. UV-Vis Spectroscopy

To examine the optical properties of as-synthesized barium oxide, UV-Visible spectroscopy was performed at room-temperature and shown in Figure 4. The sample for the

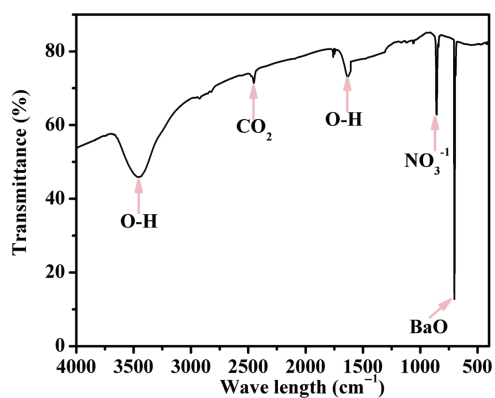


**Figure 3.** Typical FTIR spectrum of as-synthesized Barium oxide nanorods.

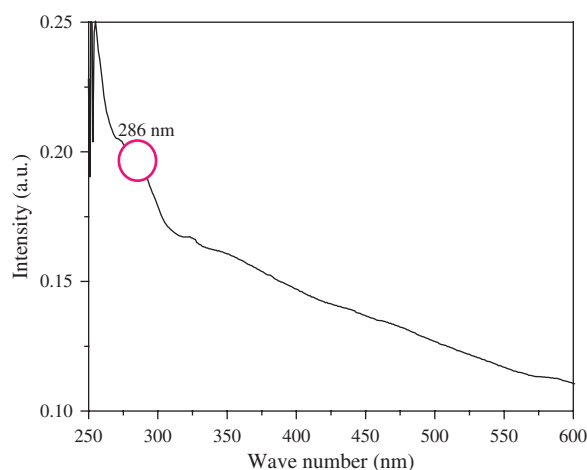


**Figure 4.** Typical UV-visible spectrum of as-synthesized Barium oxide nanorods.

UV-Visible measurement was prepared as described in literature.<sup>13,14</sup> The obtained UV-visible absorbance spectrum exhibits a well-defined excitonic absorption peak at 286 nm, which is the characteristic peak for BaO.<sup>16</sup> Except defined excitonic absorption peak, no other peak was observed in the spectrum which corroborate that the as-synthesized BaO possess good optical property.<sup>16</sup> The optical band gap energy ( $E_g$ ) of the as-synthesized BaO nanorods can be calculated by using Tauc's equation<sup>17,18</sup> which exhibits the relationship between absorption coefficient and the incident photon energy of semiconductors. The Tauc's equation is as follows:

$$(\alpha h\nu) = A(h\nu - E_g)^n$$

where  $\alpha$  is the absorption coefficient,  $h\nu$  is the photon energy,  $A$  is a constant,  $E_g$  is the optical band gap and  $n$  is a value that depends on the nature of the electronic transition responsible for the absorption ( $n = 1/2$  for direct transitions and  $n = 2$  for indirect transitions). According to the Tauc's equation, the calculated optical band gap of as-synthesized BaO nanorods is found to be 4.33 eV.<sup>16</sup> The obtained optical band gap is almost similar to the bulk BaO and consistent with the reported literature.

### 3.5. Thermo-Gravimetric Analysis (TGA)

The thermo-gravimetric analysis is used to describe the weight loss with respect to the temperature as a function. By this technique, the sample can be analysed quantitatively and qualitatively over a substantial temperature range.<sup>19</sup> Figure 5 shows the weight loss with respect to temperature of as-grown BaO nanorods. The primary weight loss or solvent evaporation point was observed at 225 °C and at this point the weight loss was  $\sim 0.94\%$  whereas at the temperature increases and reached to the optimum value. The stability of the material or secondary weight loss was observed at  $\sim 5.558\%$  (Fig. 5).

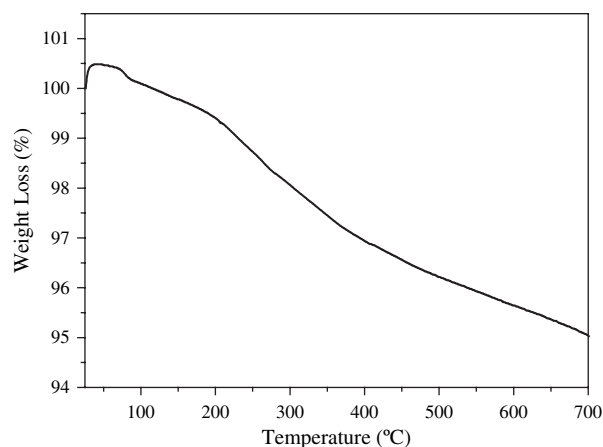
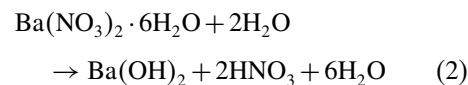
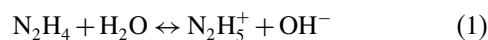


Figure 5. Typical TGA curve of as-synthesized Barium oxide nanorods.

### 3.6. Plausible Growth Mechanism of As-Synthesized Barium Oxide Nanorods

The precipitation/solution process is an aqueous chemical reaction technique by which various types of materials such as composite, organic-inorganic, metal oxides etc., at a relatively low temperature can be synthesized. This technique allows the incorporation of organic and inorganic additives during the process of formation of materials at room temperature. Based on the solution/precipitation method, various materials have been prepared and studied.<sup>20</sup> Here, a plausible growth mechanism for the formation of BaO nanorods grown at very low refluxing temperature ( $\sim 60^\circ\text{C}$ ) has been discussed. During the precipitation/solution process, hydrazine played an important role in the nucleation and growth of the BaO nanorods. During the synthesis process, in the reaction solution, hydrazine provides the hydroxyl ( $\text{OH}^-$ ) ions and hence forms a chemical equilibrium between hydroxyl ( $\text{OH}^-$ ) and  $\text{N}_2\text{H}_5^+$  ions as described in the Eq. (1).<sup>21</sup> When the reaction temperature increases up to  $\sim 60^\circ\text{C}$ , the  $\text{N}_2\text{H}_5^+$  ions can interchange into the  $\text{N}_2\text{H}_4$  and  $\text{H}^+$  ions. It is well

known that in the aqueous media barium nitrate exist in the form of  $\text{Ba}(\text{OH})_2$  and nitric acid ( $\text{HNO}_3$ ) as mentioned in Eq. (2) and in solution/precipitation process, the hydroxyl ions ( $\text{OH}^-$ ) from barium hydroxide according to the chemical reaction described in Eq. (3):



As per the reaction mechanism and the experimental observations, it is expected that as hydrazine hydrate mixed in an aqueous solution of barium nitrate, the ions of  $\text{Ba}^{2+}$  reacted with hydrazine and formed hydrazine complex  $[\text{Ba}(\text{N}_2\text{H}_4)_2]^{2+}$ . Due to unstable nature of the compound it continuously changes into  $\text{Ba}(\text{OH})_2$  and hydrazine  $[\text{N}_2\text{H}_4]$ . In an aqueous solution hydroxyl ( $\text{OH}^-$ ) ions continuously reacted with the divalent  $[\text{Ba}(\text{OH})_2]$  and form a building block of  $\text{Ba}(\text{OH})_4^{2+}$  and  $\text{H}^+$  as described in Eq. (4). As prolong refluxing temperature, the  $\text{Ba}(\text{OH})_4^{2+}$  changes into BaO and hydroxyl ions  $\text{OH}^-$  as mentioned in Eq. (5).

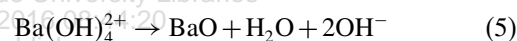
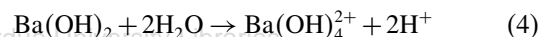


Figure 6 shows the schematic for the formation of BaO nanorods. In the first step, the aqueous solutions of barium nitrate and hydrazine were stirred for 30 min at room-temperature which was transferred to two-necked refluxing pot and was refluxed for 3 h. It is assumed that during this time the primary active nuclei were formed (Fig. 6(a)) which were the building blocks for the formation of the final products. After the nuclei formation the base of BaO

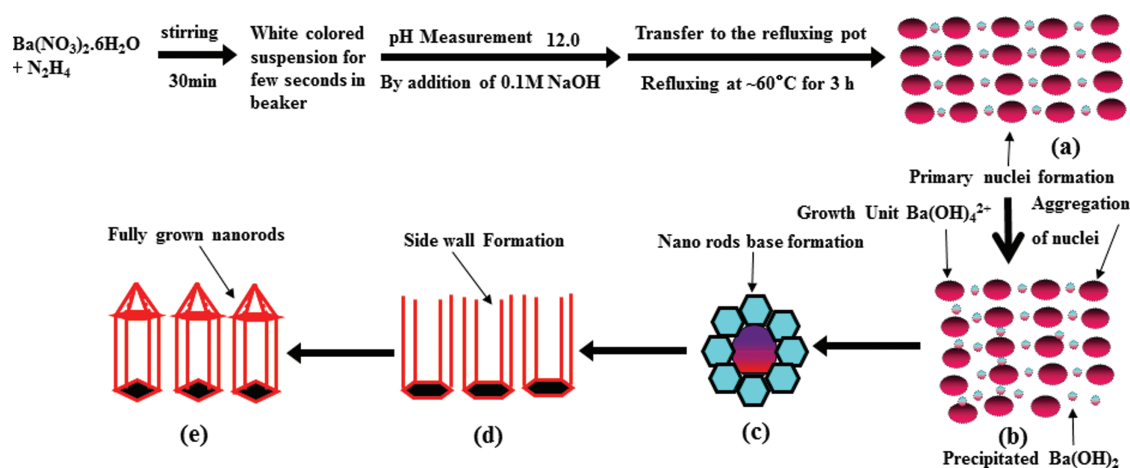


Figure 6. Typical schematic growth mechanism of barium oxide nanorods: (a) primary nuclei (b) precipitated nuclei (c) base of nanorods (d) side walls and (e) fully grown nanorods formation.

were started to form (Figs. 6(b) and (c)). It is well known that the base of newly formed crystal increases linearly with time after nuclei formation. As the new crystals grow, phase boundaries also increases at a given speed and eventually touch each other, forming the base of structure. Once the bases of nanorods were formed, growth rate start to decrease along the transverse direction and growth in the radial direction continues being the top surface an energetically favored surface (Fig. 6(c)).<sup>22</sup> After the base formation, the formed nuclei were deposited on the base and grows in liner direction (Fig. 6(d)) and changes into fully grown nanorods (Fig. 6(e)). Even though a plausible growth mechanism for the formation of BaO nanorods have been presented here, however, to understand the exact growth process further studies are needed.

#### 4. CONCLUSION

In summary, well-crystalline barium oxide nanorods were synthesized by facile solution process at low-temperature of 60 °C and characterized in detail by using various analytical tools. The detailed morphological characterization by SEM confirmed that the nanorods possess smooth and clean surfaces and are grown in very high density. The structural and compositional studies reveal that the synthesized nanorods are well-crystalline and pure without any significant impurity. Thermogravimetric analysis shows good thermal stability for the as-synthesized BaO nanorods. The nanorods exhibited good optical properties as was confirmed from the room-temperature UV-vis spectroscopy. Moreover, to understand the growth process of as-synthesized BaO nanorods, a plausible growth mechanism has also been proposed in this paper. The proposed synthesis technique can also be used for the formation of other metal oxide nanomaterials.

**Acknowledgment:** Rizwan Wahab would like to extend the appreciation to the Deanship of Scientific Research at King Saud University for funding the work through the research group project no. RGP-VPP-218.

#### References and Notes

1. Ed. A. Umar and Y. B. Hahn, *Metal Oxide Nanostructures and Their Applications*, American Scientific Publishers (ASP), Los Angeles, USA (2010).
2. M. I. Baraton, *Synthesis, Functionalization and Surface Treatment of Nanoparticles*, American Scientific Publishers, Los-Angeles, CA (2002); (b) W. J. E. Beek, M. M. Wienk, M. K. Emerink, X. Yang, and R. A. J. Janssen, *J. Phys. Chem. B* 109, 9505 (2005); (c) C. Cao, C. Hu, W. Shen, S. Wang, H. Liu, and J. Wang, *Sci. Adv. Mater.* 5, 1256 (2013).
3. (a) M. Valdivieso and M. Soustell, *Chem. Eng. Sci.* 51, 2535 (1996); (b) L. Wang, S. Tang, and H. Zhou, *Sci. Adv. Mater.* 5, 822 (2013); (c) F. Liu, J. Zhu, and D. Xue, *Sci. Adv. Mater.* 5, 904 (2013).
4. U. Manzoor and D. K. Kim, *Scripta Mater.* 54, 807 (2006).
5. X. Wang, B. I. Lee, M. Z. Hu, E. A. Payzant, and D. A. Blom, *J. Mater. Sci. Lett.* 22, 557 (2003).
6. X. Duan, Y. Huang, R. Agarwal, and C. M. Lieber, *Nature* 421, 241 (2003).
7. (a) M. H. Hung, S. Mao, H. Feick, H. Yan, Y. Wu, W. E. Kind, R. Russo, and P. Yang, *Science* 292, 1897 (2001); (b) L. Tian, C. Gong, J. Liu, L. Ye, and L. Zan, *Sci. Adv. Mater.* 5, 1627 (2013).
8. D. W. Michal, *Nature* 405, 293 (2000).
9. S. Wolf, *Microchip Manufacturing*, Lattice Press, Sunset Beach (2004).
10. J. Q. Qi, T. Peng, Y. M. Hu, L. Sun, Y. Wang, W. P. Chen, L. T. Li, C. W. Nan, and H. L. W. Chan, *Nanoscale Res. Lett.* 6, 466 (2011).
11. R. Heyding and S. Segel, *Queens University, Kingston, Canada, Private Communication* (1986).
12. P. Scherrer, *Nachr. Ges. Wiss. Göttingen* 26, 98(1918).
13. (a) M. S. Chauhan, R. Kumar, A. Umar, S. Chauhan, G. Kumar, M. Faisal, and S. W. Hwang, *J. Nanosci. Nanotechnol.* 11, 4061 (2011); (b) J. Wang, F. Qu, and X. Wu, *Sci. Adv. Mater.* 5, 1364 (2013).
14. R. Wahab, Y. S. Kim, D. S. Lee, J. M. Seo, and H. S. Shin, *Sci. Adv. Mater.* 2, 35 (2010).
15. R. Wahab, S. K. Tripathy, H. S. Shin, M. Mohapatra, J. Musarrat, A. A. Al-Khedhairi, and N. K. Kaushik, *Chem. Engg. J.* 226, 154 (2013).
16. G. Suresh and P. N. Nirmala, *Turk. J. Phys.* 36, 392 (2012).
17. W. Zhao, X. Song, Z. Yin, C. Fan, G. Chen, and S. Sun, *Mater. Res. Bull.* 43, 3171 (2008).
18. Q. Xiang, J. Yu, W. Wang, and M. Jaroniec, *Chem. Commun.* 47, 6906 (2011).
19. T. Hatakeyama and Z. Liu, *Hand Book of Thermal Analysis*, John Wiley and Sons, Ltd., Chichester, England (1998).
20. R. Wahab, S. G. Ansari, Y. S. Kim, H. K. Seo, and H. S. Shin, *Appl. Surf. Sci.* 253, 7622 (2007).
21. R. Wahab, S. G. Ansari, H. K. Seo, Y. S. Kim, E. K. Suh, and H. S. Shin, *Solid State Sci.* 11, 439 (2009).
22. R. A. Vaia, R. K. Teukolsky, and E. P. Giannelis, *Chem. Mater.* 6, 1017 (1994).

Received: 17 August 2013. Accepted: 4 September 2013.